Anisotropy of synthetic quartz electrical conductivity at high pressure and temperature

Duojun Wang,[1,2] Heping Li,[1] Li Yi,[3] Takuya Matsuzaki,[4] and Takashi Yoshino[4]

Received 14 June 2009; revised 25 November 2009; accepted 28 January 2010; published 28 September 2010.

[1] AC measurements of the electrical conductivity of synthetic quartz along various orientations were made between 0.1 and 1 MHz, at ~855~1601 K and at 1.0 GPa. In addition, the electrical conductivity of quartz along the *c* axis has been studied at 1.0–3.0 GPa. The impedance arcs representing bulk conductivity occur in the frequency range of 10^3–10^6 Hz, and the electrical responses of the interface between the sample and the electrode occur in the 0.1~10^3 Hz range. The pressure has a weak effect on the electrical conductivity. The electrical conductivity experiences no abrupt change near the $\alpha - \beta$ phase transition point. The electrical conductivity of quartz is highly anisotropic; the electrical conductivity along the *c* axis is strongest and several orders of magnitude larger than in other directions. The activation enthalpies along various orientations are determined to be 0.6 and 1.2 eV orders of magnitude, respectively. The interpretation of the former is based on the contribution of alkali ions, while the latter effect is attributed to additional unassociated aluminum ions. Comparison of determined anisotropic conductivity of quartz determined with those from field geophysical models shows that the quartz may potentially provide explanations for the behavior of electrical conductivity of anisotropy in the crust that are inferred from the transverse magnetic mode.

Citation: Wang, D., H. Li, L. Yi, T. Matsuzaki, and T. Yoshino (2010), Anisotropy of synthetic quartz electrical conductivity at high pressure and temperature, *J. Geophys. Res.*, *115*, B09211, doi:10.1029/2009JB006695.

1. Introduction

[2] Electrical conductivity is an important geophysical parameter that is used to infer physical and chemical properties in the Earth's interior, such as temperature, melt and water content, and anisotropic fabric [*Waff*, 1974; *Evans et al.*, 2005; *Simpson and Tommasi*, 2005; *ten Grotenhuis et al.*, 2005; *Karato*, 1990; *Wang et al.*, 2006, 2008; *Schock et al.*, 1989; *Wanamaker and Duba*, 1993; *Du Frane et al.*, 2005]. On the one hand, geophysical observations from magnetotelluric (MT) and geomagnetic depth sounding (GDS) may provide information on distributions of electrical conductivity in the Earth's interior; on the other hand, to interpret these field observations, laboratory measurements of electrical conductivity of minerals are conducted extensively at high pressure and temperature.

[3] Quartz is one of most abundant minerals in the Earth's crust; hence, evaluation of the conductivity distribution in the crust required more detailed information, primarily about quartz. Electrical conductivity measurements on synthetic as well as natural quartz have been conducted extensively [*Verhoogen*, 1952; *Wenden*, 1957; *Kats*, 1962; *Nowick and Jain*, 1980; *Jain and Nowick*, 1982; *Kronenberg and Kirby*, 1987; *Lazzari et al.*, 1988; *Campone et al.*, 1995; *Calleja et al.*, 2001; *Wang et al.*, 2002; *Bagdassarov and Delépine*, 2004]. These studies revealed that the electrical conductivity of quartz is ionic at temperatures above 500 K. The theoretical model of the ionic conductivity of quartz was first suggested by *Nowick and Jain* [1980] and later modified by *Jain and Nowick* [1982] and *Lazzari et al.* [1988]. One important finding from these studies is that the conduction mechanism is influenced by the presence of $(Al^{3+}\text{-}M^{+})^{-}$ centers, likely substituting for Si^{4+} and ionic impurities M^{+}, composed of Na, K, or H. However, discrepancies have been found both in the absolute values of electrical conductivity and activation energies for conductivity in previous studies. Most previous studies on electrical conductivity of quartz have been performed at 1 atm and temperatures below 773 K. *Xu et al.* [2000a] argued that the measurements of electrical conductivity at 1 atm may underestimate the absolute values of half orders of magnitude compared to measurements taken at high pressure. In addition, few studies determined the hydrogen content in their samples before and after the experiment, which may be found as a trace impurity; thus, it is still unclear whether hydrogen influences the electrical conductivity of quartz. Recently, a few measurements have been investigated at high pressure and temperature. In particular, *Bagdassarov and Delépine*

[1]Laboratory for Study of the Earth's Interior and GeoFluids, Institute of Geochemistry, Chinese Academy of Sciences, Guiyang, China.
[2]College of Earth Sciences, Graduate University of Chinese Academy of Sciences, Beijing, China.
[3]Institute of Earthquake Science, China Earthquake Administration, Beijing, China.
[4]Institute for Study of the Earth's Interior, Okayama University, Misasa, Japan.

0148-0227/10/2009JB006695

[2004] studied electrical conductivity of polycrystalline quartz in the pressure range of 0.5 to 2.5 GPa. However, this study provides the isotropic electrical conductivity and ignores the electrical conductivity anisotropy of quartz. Previous studies [*Kolodieva and Firsova*, 1969] indicated that the electrical conductivity of quartz is anisotropic; with $\sigma_{\parallel}/\sigma_{\perp} > 10^3$, where $\parallel$ and $\perp$ refer to directions parallel and perpendicular to the *c* axis. Unfortunately, there are several flaws in these studies. First, these measurements were taken using a DC method at 1 atm. Second, such studies are limited to orientations along the *c* axis or perpendicular to the *c* axis, and there is little knowledge about the conductivity at intermediate directions. Thus far, a systemic study of the anisotropy of electrical conductivity of quartz at high temperature and pressure has not been reported. Finally, although it is well known that alkali ions move in the channel parallel to the *c* axis, one remaining question in the previous studies is identification of the conduction mechanism in the quartz along directions other than the *c* axis.

[4] The high-low quartz transition from trigonal to hexagonal has been fully studied [*Coe and Paterson*, 1969; *Dolino*, 1990; *Cohen and Klement*, 1967; *Mirwald and Massonne*, 1980]. This transition may influence many physical properties of quartz-bearing rocks, such as elastic wave velocity and Poisson ratio. *Kern* [1979] investigated the effect of high-low quartz transition on compressional wave velocities in rock under high pressure; the study's results indicated that the compressional velocities of quartz decrease markedly when approaching the transition and increase markedly with temperature increase after the transition. This study concluded that the alpha-beta transition may create a low-velocity layer in the crust. In contrast, the effect of this transition on electrical conductivity remains controversial. *Gao et al.* [1998] indicated that this transition significantly affects the electrical conductivity of quartz-bearing rocks; however, some researchers have determined that this transition has little effect on the electrical conductivity. The available data under high pressure are extremely limited.

[5] In this study, we measured the electrical impedance of quartz cut at various angles to the *c* axis at 1 GPa and ~855~1601 K. We also analyzed the impedance spectra within the frequency range from 10^6 to 0.01 Hz and attempted to provide a clue to the anisotropy of the crust.

2. Experimental Procedures

2.1. Sample Preparation

[6] The starting materials were synthetic quartz crystals, which were prepared by the Bright Corp. Ltd. in China. A series of quartz cylinders were cut at various angles relative to the *c* axis, such as 0°, 20°, 35°, 49°, 57°, and 66°. The orientations of these quartz samples were determined through the use of X-ray methods and corrected to within 15″ of the desired direction during polishing. The samples were ~6.0 mm in diameter with thicknesses of ~5.0 mm.

[7] Chemical analysis of these crystals was determined by atomic absorption spectrograph, which found that the chemical compositions of impurities in quartz (by weight of atoms) are 520 ppm for Al^{3+}, 250 ppm for K^+, 310 ppm for Na^+, and 24 ppm for Li^+. The water content dissolved in the structure of the crystal was determined by infrared spectra both before and after experiment at the Institute for Study of the Earth's Interior, Okayama University, Misasa, Japan. The water content was calculated using *Paterson*'s [1982] calibration from FTIR absorption. The water content calculated in our samples was quite low, just a few parts per million.

2.2. Experiment Methods

[8] The assembly method of samples for conductivity measurements is shown in Figure 1. The cubic pyrophyllite (32 mm × 32 mm × 32 mm) used as the pressure medium was sintered at 1173 K to eliminate the potential effects of its dehydration in the experiment process. The Al_2O_3 insulating tube was placed at the center of the heater to avoid the effect of the temperature gradient. The furnaces were made of three layers of stainless steel foils connected to the ground to shield them from outer electromagnetism noise. Pt and Au electrodes were used in the experiments. A Mo shield was also used to minimize leakage currents through the pressure medium, shield the samples from electrical disturbances, and reduce temperature gradients.

[9] All the experiments were carried out in the YJ-3000 cubic-anvil high-pressure apparatus at the Institute of Geochemistry, Chinese Academy of Sciences. The apparatus has been described in detail elsewhere [*Xu et al.*, 1994; *Wang et al.*, 2008]. The temperatures of the samples were monitored by a Pth_{10}-Pt thermocouple placed against the sample. The complex impedance measurements were performed using a Solartron 1260 impedance phase analyzer. The 1 V sine signal was applied in the frequency range of 0.1 to 10^6 Hz in high temperature and pressure experiments. The semicircle that occurs in the high-frequency range in the impedance plane can be modeled using an equivalent circuits composed of a resistor in parallel with a capacitor.

3. Results and Discussion

[10] The real and imaginary elements of impedance for quartz at high pressure and temperature are acquired from amplitude and phase measured at a given frequency using the following equations:

$$Z' = |Z| \cos\theta, \tag{1}$$

$$Z'' = |Z| \sin\theta. \tag{2}$$

A typical set of complex impedance measurements is shown in Figures 2 and 3. Figure 2 shows the results of the measured parameter modules and phase angles plotted against frequency for different temperatures. The phase angles display a strong dependence on frequency, while the impedance modules decrease across the entire frequency spectrum.

[11] A complex plane plot, which is a plot of the imaginary part against the real part of the complex impedance, is shown in Figure 3. At a given temperature, the complex impedance plot maps out an arc at high frequencies and becomes linear at lower frequencies. The arched and linear regions correspond to two separate conduction mechanisms that are dominant at different frequency ranges and exhibit different relaxation times ($\tau = R \times C$). In the complex impedance plane, the electrode response appears as an arc or straight line at low frequency, which is characteristic of dif-

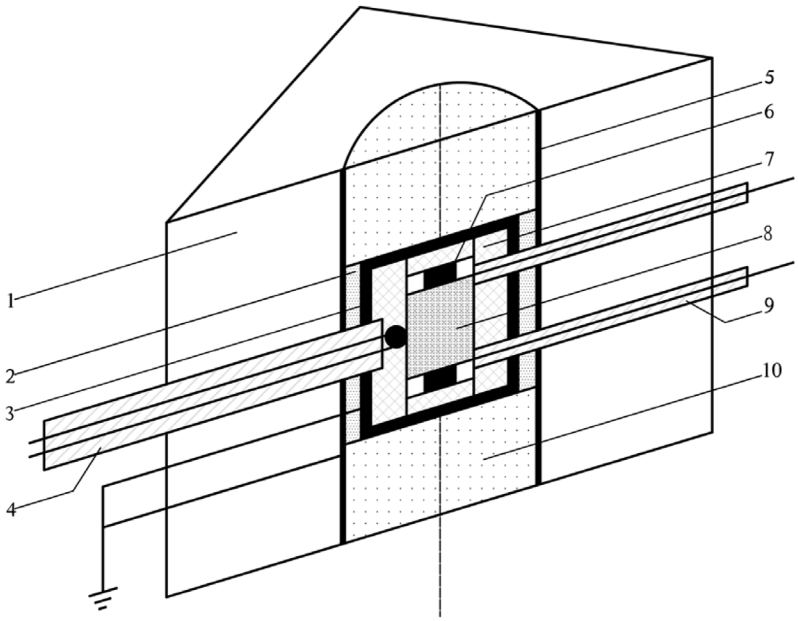

Figure 1. Sample assembly for electrical conductivity measurements at high pressure. (1) Pyrophyllite (baked to 1073 K); (2) Pyrophyllite sleeve (baked to 1273 K); (3) Mo shield; (4) Thermocouple; (5) Furnace; (6) Electrode; (7) Al_2O_3 sleeve; (8) Sample; (9) Electrical wire; (10) Pyrophyllite cylinder (baked to 1273 K).

fusion processes at the sample-electrode interface. Previous studies [*Tyburczy and Roberts*, 1990; *Roberts and Tyburczy*, 1991, 1993a, 1993b, 1994; *Huebner and Dillenaurg*, 1995; *Xu et al.*, 2000b] have indicated that a high-frequency arc represents bulk properties of the sample.

[12] The bulk direct current conductivity of the sample is calculated according to the following equation:

$$\sigma_{\text{bulk}} = \frac{L}{RS}, \tag{3}$$

where S is the cross-sectional area, L is the sample thickness, and R is the bulk DC resistance of the sample.

[13] To test the effect of types of electrodes used on the absolute electrical conductivity values, Au electrodes and Pt electrodes were used, respectively. The results are shown in Figure 4. The results show good reproduction in both experiments, which implies that the electrical electrodes have only a weak effect on bulk electrical conductivity of quartz in this study.

[14] Figure 5 shows the electrical conductivity along the c axis at 1–3 GPa. It can be seen that the pressure has a weak effect on electrical conductivity. The results agree well with previous research [*Xu et al.*, 2000b; *Bagdassarov and Delépine*, 2004; *Katsura et al.*, 2007]. The activation

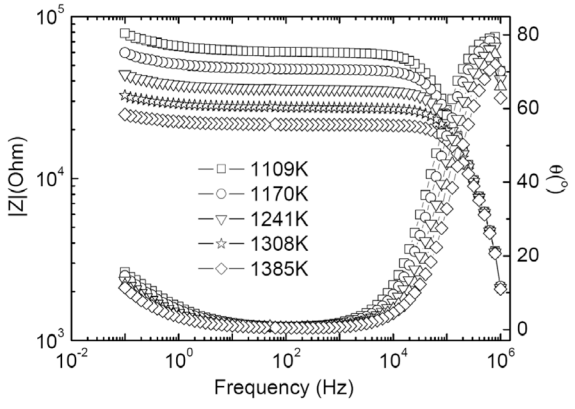

Figure 2. Modules and phase angles plotted against frequency along $Z35$ at various temperatures at 1.0 GPa. These symbols represent modules, $|Z|$, and angles, θ, at various temperatures.

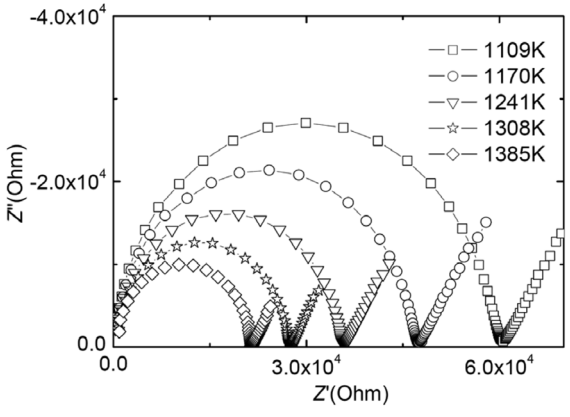

Figure 3. Complex impedance arcs along $Z35$ at various temperatures at 1.0 GPa. These symbols represent impedance arcs at different temperatures at 1.0 GPa. The frequency of each data point increases from right to left along each trajectory.

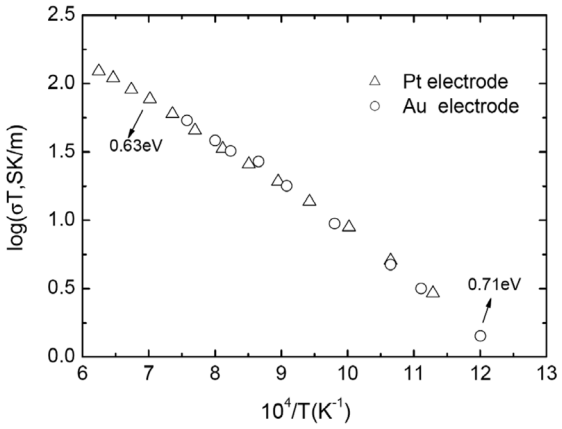

Figure 4. Logarithm of electrical conductivity as a function of reciprocal temperature for quartz parallel to the *c* axis using different electrodes at 1.0 GPa.

energy and activation volume were calculated through polybaric fitting to all the electrical data at various pressures according to the following equation:

$$\sigma T = A \exp(-\Delta H/\kappa T), \tag{4}$$

where A, the preexponential factor, and ΔH, the activation enthalpy, are experimentally determined quantities; $\Delta H = \Delta U + P\Delta V$, where ΔU is activation energy and ΔV is the activation volume; κ is the Boltzmann constant; and T is the absolute temperature. The determined activation energy and activation volume are 0.71 ± 0.01 eV and 0.59 ± 0.14 cm^3/mole, respectively.

[15] The electrical conductivity of quartz across various orientations at 1.0 GPa was investigated. The results are summarized in Figure 6. In the same figure, we have also indicated the temperature T = 1099 K, at which point the transition from α to β quartz at 1.0 GPa is predicted to occur, according to the following equation [*Mirwald and Massonne*, 1980]:

$$T = 847.3 + 271.084P - 23.607P^2 + 3.91P^3, \tag{5}$$

where T is measured in kelvins and P is measured in gigapascals. The activation enthalpies and preexponential factor A, in accordance with equation (4), are listed in Table 1.

[16] From Figure 6, we can see that the electrical conductivity of quartz exhibits no abrupt change near the alpha-beta phase transition. This result is in accordance with that found by *Bagdassarov and Delépine* [2004] when polycrystalline samples were pressed from powder of natural SiO_2 quartz at 0.5–2.5 GPa. However, our results are not consistent with the results reported by *Gao et al.* [1998]. These researchers studied electrical conductivity of quartz-bearing rocks in the middle-lower crust, such as gneiss, granulite, and eclogite, and their results showed that quartz can lead to a decrease in electrical conductivity among these rocks with the values of 0.1–0.001 S/m due to the alpha- to beta-phase transition in quartz under the pressure and temperature conditions of the lower crust. We argue that the electrical conductivity has no abrupt change near the alpha- to beta-phase transition, since the cross section of the channels along the *c* axis at the inversion temperature only changes slightly (~3.4%) [*Bagdassarov and Delépine*, 2004]. This result is consistent with the fact that this transition does not produce a significant change in the radius of the *c* axis.

[17] From Figures 6 and 7, it can be seen that electrical conductivity is greatest in the *c* axis at a given temperature; the electrical conductivity drops significantly with the increase in the angle to *c* axis, suggesting that the electrical conductivity of quartz is influenced by the radius of the channel along the optical axis. The slopes of the electrical conductivity curves along 49°, 57°, and 66° increase signif-

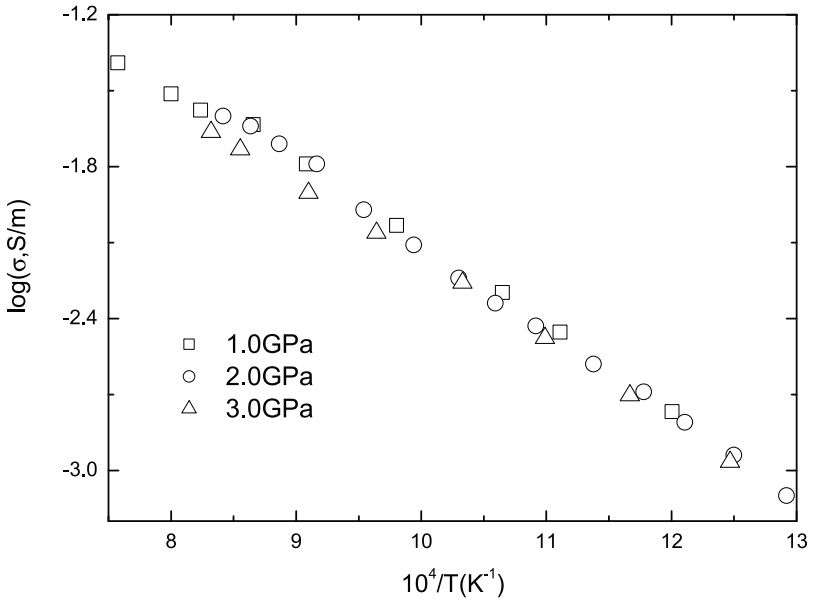

Figure 5. Logarithm of electrical conductivity versus reciprocal temperature for quartz parallel to the *c* axis at 1.0, 2.0, and 3.0 GPa.

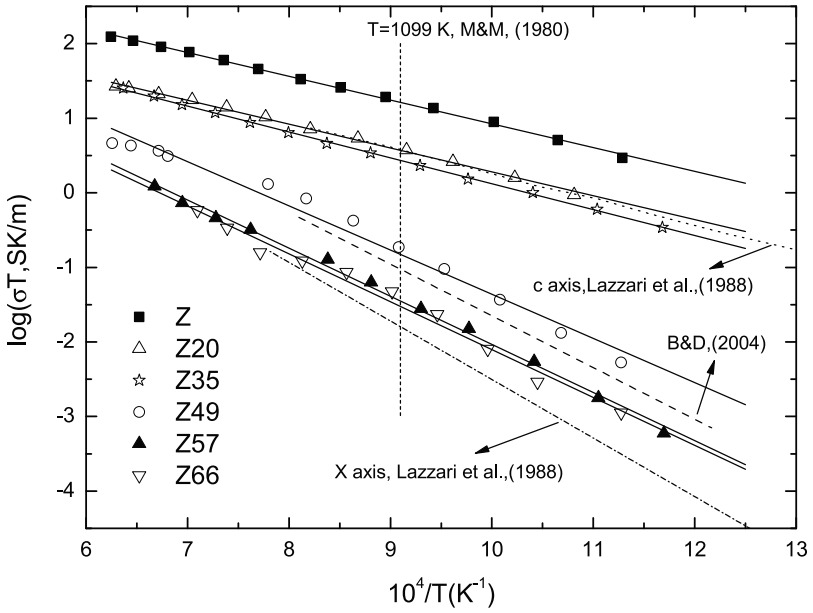

Figure 6. Logarithm of electrical conductivity as a function of reciprocal temperature for quartz along various orientations at 1.0 GPa. *Z* denotes the *c* axis; *Z*20, *Z*35, *Z*49, *Z*57, and *Z*66 represent the directions inclined 20°, 35°, 49°, 57°, and 66° relative to the *c* axis, respectively. The short-dashed lines show the temperature $T = 1099$ K, where the transition from alpha to beta quartz occurs at 1.0 GPa [*Mirwald and Massonne*, 1980].The dotted lines and dash-dotted lines indicate the electrical conductivity of quartz parallel and perpendicular to the *c* axis [*Lazzari et al.*, 1988]. Long-dashed lines show the electrical conductivity of polycrystalline quartz at 1.0 GPa [*Bagdassarov and Delépine*, 2004].

icantly, showing that at least two conduction mechanisms are operative. Figure 7 shows the anisotropy of the electrical conductivity at different temperatures; we can see that the electrical conductivity of quartz shows high anisotropy and that the maximum degree of anisotropy is as high as 10,000. The anisotropy of the electrical conductivity is temperature dependent and decreases with increasing of temperature. For example, the electrical conductivity along the *c* axis is about 1.5 and 4.0 times larger than that along the Z66 direction at 800 and 1600 K, respectively. Previous studies [*Kolodieva and Firsova*, 1969] on the electrical conductivity of quartz have indicated that the conductivity parallel to the open channels is three times larger than that perpendicular to the *c* optical axis. However, our results indicate that the anisotropy of the electrical conductivity in quartz is more complicated. Specifically, the anisotropy of electrical conductivity depends on both orientations and temperatures.

[18] In comparison with previous measurements of natural single-crystal synthetic samples oriented along the *c* axis, which have been done at atmospheric pressure, the data of the electrical conductivity obtained from previous studies are half orders of magnitude lower than that obtained on a single crystal oriented along the *c* axis and are similar to the electrical conductivity data in the *Z*20 orientation. The previous measurements [*Lazzari et al.*, 1988], which have been done on a synthetic sample oriented perpendicular to the *c* axis at high temperature, are close to the electrical conductivity results in the *Z*57 and *Z*66 orientation in this study. The recent studies on polycrystalline samples, which were pressed from powdered SiO_2, show isotropic electrical conductivity, which is a half order of magnitude higher than that in the *Z*57 orientation. Thus, we conclude that the differences in electrical conductivity between natural and samples are smaller than the anisotropy of electrical conductivity in quartz.

[19] The activation enthalpies obtained in this study are 0.6–1.2 eV (Table 1); obviously, they can be divided into two groups, suggesting that there are at least two kinds of conduction mechanisms (Figure 6) corresponding to each of the activation enthalpies of 0.6 and 1.2 eV (see Table 1).

[20] Theoretical models on the conduction mechanism in quartz parallel to the *c* axis at $T < 773$ K and $800\ \text{K} < T < 1200$ K have been presented by *Jain and Nowick* [1982] and *Lazzari et al.* [1988], respectively. They suggest the electrical conductivity of quartz is governed by the reaction

$$\left(\text{Al}^{3+} - \text{M}^{+}\right) \Leftrightarrow \text{Al}_s + \text{M}_i, \tag{6}$$

Table 1. Results for Activation Enthalpies and Pre-exponential for Synthetic Quartz at Various Orientations

Orientations	T (K)	$\log_{10} \sigma_0$	σ_0 (S/m)	ΔH (eV)
Z	886–1601	4.11 ± 0.04	12,891	0.63 ± 0.01
Z20	925–1589	3.48 ± 0.05	3,046	0.64 ± 0.01
Z35	856–1571	3.59 ± 0.02	3,952	0.69 ± 0.01
Z49	887–1598	4.57 ± 0.22	37,257	1.18 ± 0.05
Z57	855–1498	4.42 ± 0.11	26,144	1.28 ± 0.02
Z66	887–1409	4.32 ± 0.25	20,892	1.27 ± 0.05

Note: *Z* denotes the *c* axis; Z20, Z35, Z49, Z57, and Z66 represent the directions inclined 20°, 35°, 49°, 57°, and 66°, respectively, relative to the *c* axis.

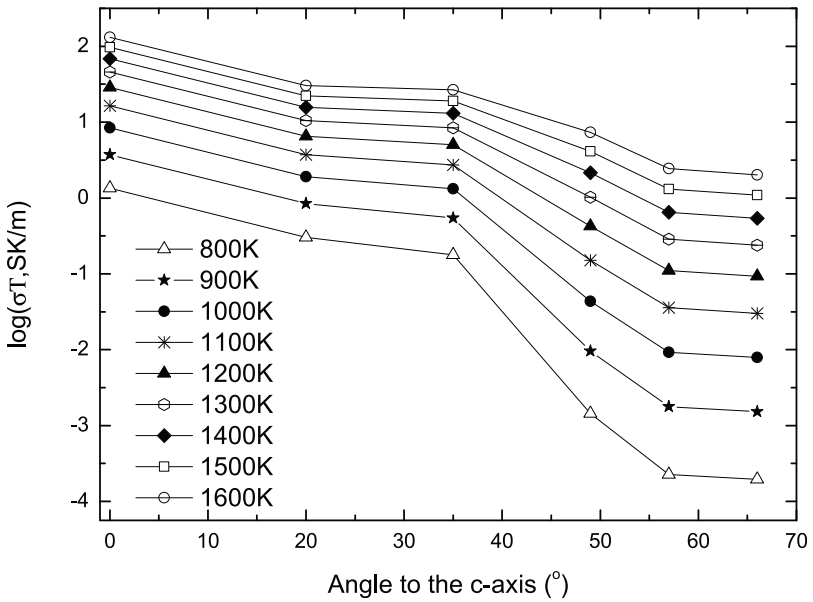

Figure 7. Logarithm of electrical conductivity as a function of angles inclined to the *c* axis from 800 K to 1600 K. These symbols represent electrical conductivities at various temperatures.

where M_i is free-interstitial alkali, and Al_s is an unassociated Al^{3+} substitutional. The quantity of alkali ions (c_i) is controlled by the mass-action relation:

$$c_i c_s / c_p = (1/2)\exp(-H_f/\kappa T), \tag{7}$$

where H_f is the enthalpy for Al–M pair formation, while c_i, c_s and, c_p are the concentrations of free alkali ions, interstitial unassociated aluminum ions, and Al-M^+ pairs, respectively. It can be seen that the Al–M pair dissociation equilibrium can be affected by the presence of additional unassociated substitutional Al. Two forms for the dependence of electrical conductivity on temperature were proposed in previous studies [*Jain and Nowick*, 1982; *Lazzari et al.*, 1988] due to the ratio between c_i and c_s; (1) If $c_i = c_s$, the conduction mechanism is governed by the alkali ions, and electrical conductivity can be expressed as

$$\sigma T = A\exp\left\{-\left(\frac{1}{2}H_f + H_M\right)/\kappa T\right\}. \tag{8}$$

Accordingly, the activation enthalpy in equation (4) becomes $\Delta H = \frac{1}{2}H_f + H_m$. (2) If $c_s \gg c_i$, the conduction mechanism is controlled by additional unassociated aluminum ions; thus, the electrical conductivity can be expressed as

$$\sigma T = A\exp\{-(H_f + H_M)/\kappa T\}, \tag{9}$$

and the activation enthalpy in the equation (4) is $\Delta H = H_f + H_m$.

[21] In our case, under conditions of 1.0 GPa, activation enthalpy of the bulk conduction for charge carriers in quartz parallel to the *c* axis is 0.63 eV. This value is similar to the experiments (0.67 eV) of *Lazzari et al.* [1988] on activation enthalpy of synthetic quartz along the *c* axis, which was obtained at 1 atm and between 800 and 1200 K. This agreement between our experiments and previous studies is quite good. Indeed, the agreement suggests that our observations can be interpreted through equation (8); therefore, the conduction mechanism is the alkali ion moving in channels parallel to the *c* axis. Since the activation enthalpies oriented along the *c* axis, *Z*20, and *Z*35 are similar, we conclude that conduction mechanisms among these orientations are similar. Based on the experimentally measured activation enthalpy values (shown in Table 1) and assuming migration enthalpy of 0.14 eV [*Jain and Nowick*, 1982], we calculated formation enthalpies using equation (8); they are 0.49, 0.50, and 0.55 eV in the orientations of the *c* axis, *Z*20, and *Z*35, respectively. Along the open channels, we calculated activation enthalpies of 0.6–0.7 eV.

[22] However, the activation enthalpies in the present study are smaller than the results (>1.2 eV) from both *Jain and Nowick* [1982] and *Xu et al.* [1989] on synthetic single quartz and amorphous SiO_2 under conditions of 1 atm and 450–773 K, and the results (>1.2 eV) of *Bagdassarov and Delépine* [2004] on polycrystalline quartz under conditions of 0.5–2.5 GPa and 800–1000 K. These differences between our results and previous studies [*Jain and Nowick*, 1982; *Bagdassarov and Delépine*, 2004; *Wang et al.*, 2002] were caused by the fact that the narrow and lower temperature ranges were used to determine the activation enthalpy in the experiments of single crystals by *Jain and Nowick* [1982] and *Wang et al.* [2002], and that the polycrystalline crystals with random orientations were measured in the study by *Bagdassarov and Delépine* [2004]. In addition, previous studies on olivine single-crystal conductivity [*Du Frane et al.*, 2005] show that the activation enthalpy in different orientations is very different. Hence, we argue that the conduction mechanism is controlled by the temperature range and orientations.

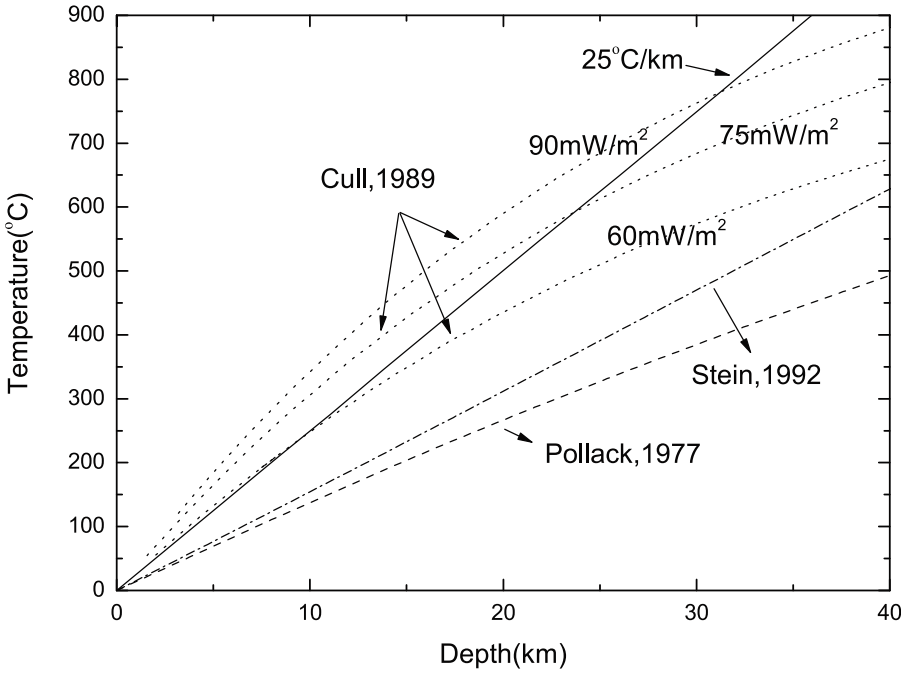

Figure 8. Several geothermic gradient models for different regions. The solid line indicates the experiential geothermic gradient with 25°C/km. The dotted lines are geothermal models constructed for Australia consistent with seismic refraction data suggested by *Cull* [1989] assuming 60, 75, and 90 mW/m^2 heat flow, respectively. The dashed line is geotherms for an old continental lithosphere assuming a 50 mW/m^2 surface heat flow by *Pollack and Chapman* [1977]. The dotted-dashed line is geotherms for an old oceanic lithosphere assuming a 50 mW/m^2 surface heat flow by *Stein and Stein* [1992].

[23] The higher activation enthalpies in the *Z*47, *Z*59, and *Z*66 orientations with values of 1.27–1.37 eV have not been reported previously. These values are close to the value (1.3 eV) along the c-axis obtained by the *Jain and Nowick* [1982] at low temperature. We attempted to interpret our results by virtue of equation (9), since alkali ions may not move freely because there are no open channels among these orientations. According to equation (9), we determined H_f to be ~1.04, 1.14, and 1.13 eV, respectively. In this case, we suggest that the electrical conductivity is controlled by the remaining unassociated aluminum ions and is no longer controlled by the alkali ions.

[24] It should be considered whether hydrogen dissociated from aluminum centers contributes to the ionic conductivity of quartz. It is well known that hydrogen influences the electrical conductivity of silicate mineral [*Karato*, 1990, 2003, 2006; *Huang et al.*, 2005; *Wang et al.*, 2006, 2008]. In this case, however, the typical FTIR spectra [*Kats*, 1962; *Paterson*, 1982] of samples at the 3000 to 4000 cm^{-1} wave number were not found; this means that our samples are dry. Since the slope of the electrical conductivity did not change throughout the whole temperature region at a fixed orientation, we concluded that the hydrogen has a weak effect on the electrical conductivity of quartz. The other supporting evidence for the above results can be found in previous experiments. *Campone et al.* [1995] pointed out that hydrogen is not a charge carrier in quartz because of the low conductivity of H-rich electrodiffuse quartz. Several researchers [*Aines et al.*, 1984; *Newton-Howes et al.*, 1989] also indicated the dominant hydrogen impurity in synthetic quartz is molecular water.

4. Geophysical Implication

[25] Electrical anisotropy beneath mid-ocean ridges, subduction zones, and cratons has been extensively observed using a magnetotelluric method [*Simpson*, 2002; *Eaton et al.*, 2004; *Evans et al.*, 2005; *Heinson and White*, 2005]. Magnetotelluric results show that electrical anisotropy factors are as high as 100 in the mantle [*Bahr and Simpson*, 2002] and perhaps up to 1000 in the lower crust [*Cull*, 1985]. More recently, *Heinson and White* [2005] suggested that the lower crust beneath the North Australian Craton is strongly anisotropic in resistivity, with anisotropy of more than 100 over depths of 20–40 km across at least 300 km of the survey line. Electrical conductivity is sensitive to factors such as orientation and temperature. Anisotropy of electrical conductivity as a result of orientation induced at high pressure and temperature is expected to provide a significantly scientific basis for interpreting these field-observed results.

[26] Figure 8 shows several geothermal gradient models. The North Australian Craton was subject to extensive continental back-arc extension between 1.8 and 1.6 Ga; the heat flow values around this region are in the range of 60–90 mW/m^2 (for details see *Cull* [1989]). *Cull* [1989] presented several geothermal models constructed for Australia consistent with seismic refraction data. We selected three temperature-depth profiles derived by *Cull* [1989] that

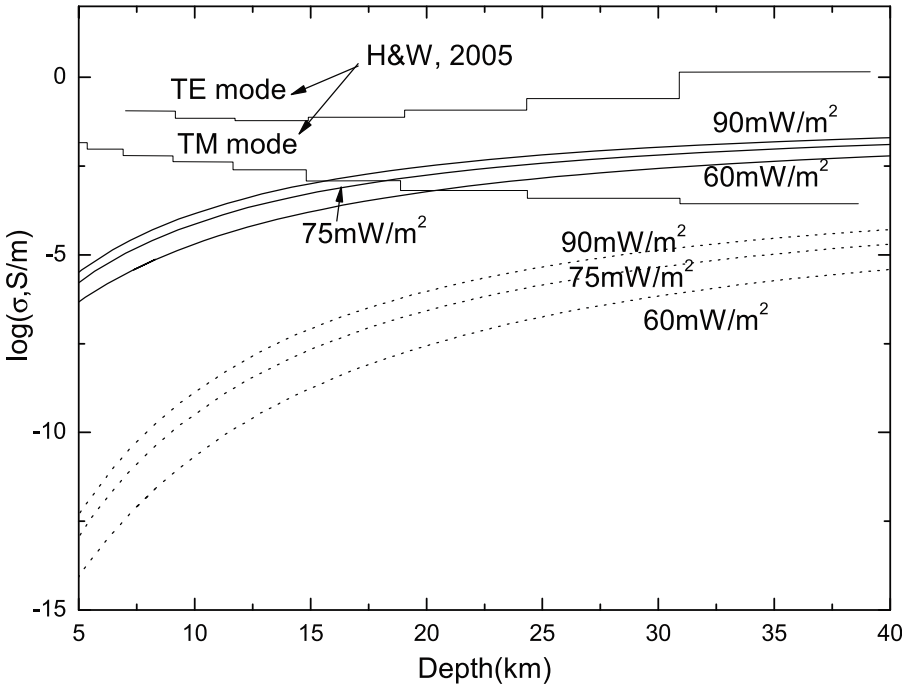

Figure 9. Comparison of laboratory-based conductivity depth with geophysically inferred electrical conductivity for the crust. Transverse electric (TE) and transverse magnetic (TM) were obtained by *Heinson and White* [2005]. Solid lines show the electrical conductivity of quartz along the *c* axis as a function of depth for geothermal models suggested by *Cull* [1989]. Short-dashed lines show the electrical conductivity of quartz perpendicular to the *c* axis. The electrical conductivity of quartz perpendicular to the *c* axis was calculated using the parameters for *Z*66 in Table 1. The numbers with lines indicate the heat flow values.

assume the heat flow values are 60, 75, and 90 mW/m^2. We calculated the electrical conductivity of quartz parallel and perpendicular (assuming that the perpendicular direction is equivalent to *Z*66) to the *c* axis according to these temperature-depth profiles and compared the results with geophysical observation of the crust by *Heinson and White* [2005]. Figure 9 shows a comparison between electrical conductivity of quartz parallel and perpendicular to the *c* axis along geothermal profiles and that inferred from MT observations. Obviously, electrical conductivity values of quartz both parallel and perpendicular to the *c* axis derived from laboratory data are much lower than those inferred from the transverse electric (TE) mode (currents flowing parallel to geologic strike). In this case, to interpret higher conductivity values, some conductive materials may be considered, such as fluid-filled or grain boundary graphite. The electrical conductivities of quartz parallel to the *c* axis are consistent with the lower limit of the transverse magnetic mode (currents flowing perpendicular to their geologic strike) at the depth of 15–40 km. We conclude that quartz may be used to interpret the observation data inferred from the TM mode in some regions. It should be noted, however, that the discrepancy between our model and geophysical observations may arise from the fact that other phases coexist in the continental crust but are neglected in our model.

5. Conclusions

[27] We have presented the electrical conductivity of quartz at 1.0 GPa in various orientations, and we have discussed conduction anisotropy and geophysical implication. Our major conclusion may be summarized as follows:

[28] 1. Electrical conductivity of quartz is influenced by temperatures and orientations. Electrical conductivity of quartz is highly anisotropic, with the maximum degree of anisotropy as high as 10,000, and the degree of the anisotropy of electrical conductivity decreasing with increases in temperature.

[29] 2. At least two conduction mechanisms occur in quartz. In higher-temperature regions and open channels, the carrier is the alkali ions corresponding to the small activation enthalpy, while in lower-temperature regions and narrow channels, the electrical conductivity is governed by the presence of the additional unassociated aluminum ions that correspond to the larger activation enthalpy.

[30] 3. Pressure plays a minor role in affecting the electrical conductivity of quartz in both the alpha and beta phases. The transition between alpha and beta cannot cause the decrease in electrical conductivity. Therefore, the transition may not offer a reasonable explanation for the occurrence of the lower conductivity layer in the lower crust.

[31] 4. Electrical conductivity of quartz parallel and perpendicular to the *c* axis along geothermal profiles is compared to that inferred from MT observations. Electrical conductivity models of quartz derived from laboratory data along geothermal gradient are generally lower than those inferred from geophysical observations.

[32] **Acknowledgments.** We thank two anonymous reviewers and an associate editor for their valuable suggestions. We also thank Karato S.-I.,

Xu Y.-S., Michael Kendall, Baoping Shi, and Han Li for helpful discussions. This work is partially supported by National Natural Science of China (40774036), Important Field Program of Knowledge Innovation Project of CAS (KZCX2-YW-Q08-3-4, XMXX280728), Special Fund for president prize of CAS, and Special Fund of Graduate University of CAS.

References

Aines, R. D., S. H. Kirby, and G. R. Rossman (1984), Hydrogen speciation in synthetic quartz, *Phys. Chem. Miner.*, *11*, 204–212, doi:10.1007/BF00308135.

Bagdassarov, N. S., and N. Delépine (2004), α-β inversion in quartz from low frequency electrical impedance spectroscopy, *J. Phys. Chem. Solids*, *65*, 1517–1526, doi:10.1016/j.jpcs.2003.10.075.

Bahr, K., and F. Simpson (2002), Electrical anisotropy below slow- and fast-moving plates: Palaeoflow in the upper mantle? *Science*, *295*, 1270–1272, doi:10.1126/science.1066161.

Calleja, M., M. T. Dove, and E. K. J. Salje (2001), Anisotropic ionic transport in quartz: The effect of twin boundaries, *J. Phys. Condens. Matter*, *13*, 9445–9454, doi:10.1088/0953-8984/13/42/305.

Campone, P., M. Magliocco, G. Spinolo, and A. Vedda (1995), Ionic transport in crystalline SiO_2: The role of alkali-metal ions and hydrogen impurities, *Phys. Rev. B*, *52*, 15903–15908, doi:10.1103/PhysRevB.52.15903.

Coe, R. S., and M. S. Paterson (1969), The alpha-beta inversion in quartz: A coherent phase transition under nonhydrostaic stress, *J. Geophys. Res.*, *74*(B20), 4921–4948, doi:10.1029/JB074i020p04921.

Cohen, L. H., and W. Klement Jr. (1967), High-low quartz inversion: Determination to 35 kilobars, *J. Geophys. Res.*, *72*(16), 4245–4251, doi:10.1029/JZ072i016p04245.

Cull, J. P. (1985), Magnetotelluric soundings over a Precambrian contact in Australia, *Geophys. J. R. Astron. Soc.*, *80*, 661–675, doi:10.1111/j.1365-246X.1985.tb05117.x.

Cull, J. P. (1989), Geothermal models and mantle rheology in Australia, *Tectonophysics*, *164*, 107–115, doi:10.1016/0040-1951(89)90004-8.

Dolino, G. (1990), The α to β transitions of quartz: A century of research on displacive phase transitions, *Phase Transit.*, *21*, 59–72, doi:10.1080/01411599008206882.

Du Frane, W. L., J. J. Roberts, D. A. Toffelmier, and J. A. Tyburczy (2005), Anisotropy of electrical conductivity in dry olivine, *Geophys. Res. Lett.*, *32*(24), L24315, doi:10.1029/2005GL023879.

Eaton, D. W., A. G. Jones, and I. J. Ferguson (2004), Lithospheric anisotropy structure inferred from collocated teleseismic and magnetotelluric observations: Great Slave Lake shear zone, northern Canada, *Geophys. Res. Lett.*, *31*(19), L19614, doi:10.1029/2004GL020939.

Evans, R. L., G. Hirth, K. Baba, D. Forsyth, A. Chave, and R. Mackie (2005), Geophysical evidence from the MELT area for compositional controls on oceanic plates, *Nature*, *437*, 249–252, doi:10.1038/nature04014.

Gao, P., P. Yang, and Y. J. Li (1998), Experimental study on the electric conductivity under high pressure and high temperature for the crust-mantel rocks in Qingling-Dabie mountain, *Sci. Geol. Sinica*, *33*, 195–203.

Heinson, G., and A. White (2005), Electrical resistivity of the northern Australian lithosphere: Crustal anisotropy or mantle heterogeneity? *Earth Planet. Sci. Lett.*, *232*, 157–170, doi:10.1016/j.epsl.2004.12.029.

Huang, X. G., Y. S. Xu, and S. I. Karato (2005), Water content in the transition zone from electrical conductivity of wadsleyite and ringwoodite, *Nature*, *434*, 746–749, doi:10.1038/nature03426.

Huebner, J. S., and R. G. Dillenaurg (1995), Impedance spectra of dry silicate minerals and rock: Qualitative interpretation of spectra, *Am. Mineral.*, *80*, 46–64.

Jain, H., and A. S. Nowick (1982), Electrical conductivity of synthetic and natural quartz crystals, *J. Appl. Phys.*, *53*, 477–484, doi:10.1063/1.329949.

Karato, S. (1990), The role of hydrogen in the electrical conductivity of the upper mantle, *Nature*, *347*, 272–273, doi:10.1038/347272a0.

Karato, S. (2003), Mapping water content in the upper mantle, in *Inside the Subduction Factory*, Geophys. Monogr., edited by J. Eiler, pp. 138,135–138,152, AGU, Washington, D. C.

Karato, S. (2006), Remote sensing of hydrogen in Earth's mantle reviews in mineralogy and geochemistry, in *Water in Nominally Anhydrous Minerals*, vol. 62, edited by H. Keppler and J. R. Smyth, pp 343–375, Mineral. Soc. Am., Washington, D. C.

Kats, A. (1962), Hydrogen in alpha-quartz, *Philips Res. Rept.*, *17*, 201–279.

Katsura, T., S. Yokoshi, K. Kawabe, A. Shatskiy, M. Okube, H. Fukui, E. Ito, A. Nozawa, and K. I. Funakoshi (2007), Pressure dependence of electrical conductivity of $(Mg,Fe)SiO_3$ ilmenite, *Phys. Chem. Miner.*, *34*, 249–255, doi:10.1007/s00269-007-0143-0.

Kern, H. (1979), Effect of high-low quartz transition on compressional and shear wave velocities in rocks under high pressure, *Phys. Chem. Miner.*, *4*, 161–171, doi:10.1007/BF00307560.

Kolodieva, S. V., and M. M. Firsova (1969), The electrical conductivity of natural and synthetic quartz in a constant electrical field, *Sov. Phys. Crystallogr.*, *13*, 540–544.

Kronenberg, A. K., and S. H. Kirby (1987), Ionic conductivity of quartz: DC time dependence and transition of charge carriers, *Am. Mineral.*, *72*, 739–747.

Lazzari, S., M. Martini, A. Paleari, G. Spinolo, and A. Vedda (1988), DC and AC ionic conductivity in quartz: A new high temperature mechanism and a general assessment, *Nucl. Instrum. Methods Phys. Res. B*, *32*, 299–302.

Mirwald, P. W., and H. J. Massonne (1980), The low-high quartz and quartz-coesite transition to 40 kbar between 600° and 1600°C and some reconnaissance data on the effect of $NaAlO_2$ component on the low quartz-coesite transition, *J. Geophys. Res.*, *85*(B12), 6983–6990, doi:10.1029/JB085iB12p06983.

Newton-Howes, J. C., A. C. McLaren, and R. J. Fleming (1989), An investigation of the effects of hydroxyl concentration and bubble formation on the electrical conductivity of synthetic quartz, *Tectonophysics*, *158*, 335–342, doi:10.1016/0040-1951(89)90331-4.

Nowick, A. S., and H. Jain (1980), Electrical conductivity and dielectric loss of quartz crystals before and after irradiation, in *Proceedings of the 34th Annual Frequency Control Symposium*, pp. 9–13, Ultrasonics, Ferroelectr., and Frequency Control Soc., Inst. of Electr. and Electron. Eng., New York.

Paterson, M. S. (1982), The determination of hydroxyl by infrared absorption in quartz, silicate glasses and similar materials, *Bull. Mineral.*, *105*, 20–29.

Pollack, H. N., and D. S. Chapman (1977), On the regional variation of heat flow, geotherms, and the thickness of the lithosphere, *Tectonophysics*, *38*, 279–296, doi:10.1016/0040-1951(77)90215-3.

Roberts, J. J., and J. A. Tyburczy (1991), Frequency dependent electrical properties of polycrystalline olivine compacts, *J. Geophys. Res.*, *96*(B10), 16,205–16,222, doi:10.1029/91JB01574.

Roberts, J. J., and J. A. Tyburczy (1993a), Impedance spectroscopy of single and polycrystalline olivine: Evidence for grain boundary transport, *Phys. Chem. Miner.*, *20*, 19–26, doi:10.1007/BF00202246.

Roberts, J. J., and J. A. Tyburczy (1993b), Frequency dependent electrical properties of dunite as functions of temperature and oxygen fugacity, *Phys. Chem. Miner.*, *19*, 545–561, doi:10.1007/BF00203054.

Roberts, J. J., and J. A. Tyburczy (1994), Frequency dependent electrical properties of minerals and partial-melts, *Surv. Geophys.*, *15*, 239–262, doi:10.1007/BF00689861.

Schock, R. N., A. G. Duba, and T. J. Shankland (1989), Electrical conduction in olivine, *J. Geophys. Res.*, *94*(B5), 5829–5839, doi:10.1029/JB094iB05p05829.

Simpson, F. (2002), Intensity and direction of lattice-preferred orientation of olivine: Are electrical and seismic anisotropies of the Australian mantle reconcilable? *Earth Planet. Sci. Lett.*, *203*, 535–547, doi:10.1016/S0012-821X(02)00862-2.

Simpson, F., and A. Tommasi (2005), Hydrogen diffusivity and electrical anisotropy of a peridotite mantle, *Geophys. J. Int.*, *160*, 1092–1102, doi:10.1111/j.1365-246X.2005.02563.x.

Stein, C. A., and S. Stein (1992), A model for the global variation in oceanic depth and heat flow with lithospheric age, *Nature*, *359*, 123–129, doi:10.1038/359123a0.

ten Grotenhuis, S. M., M. R. Drury, C. J. Spiers, and C. J. Peach (2005), Melt distribution in olivine rocks based on electrical conductivity measurements, *J. Geophys. Res.*, *110*(B12), B12201, doi:10.1029/2004JB003462.

Tyburczy, J. A., and J. J. Roberts (1990), Low frequency electrical response of polycrystalline olivine compacts: Grain boundary transport, *Geophys. Res. Lett.*, *17*(11), 1985–1988, doi:10.1029/GL017i011p01985.

Verhoogen, J. (1952), Ionic diffusion and electrical conductivity in quartz, *Am. Mineral.*, *37*, 637–655.

Waff, H. S. (1974), Theoretical considerations of electrical conductivity in a partially molten mantle and implications for geothermometry, *J. Geophys. Res.*, *79*(B26), 4003–4010, doi:10.1029/JB079i026p04003.

Wanamaker, B. J., and A. G. Duba (1993), Electrical conductivity of San Carlos olivine along [100] under oxygen- and pyroxene-buffered conditions and implications for defect equilibria, *J. Geophys. Res.*, *98*(B1), 489–500, doi:10.1029/92JB01584.

Wang, D., H.-P. Li, C. Q. Liu, L. Yi, D. Y. Ding, G. L. Su, and W. G. Zhang (2002), Electrical conductivity of synthetic quartz crystals at high temperature and pressure from complex impedance measurements, *Chin. Phys. Lett.*, *19*, 1211–1213, doi:10.1088/0256-307X/19/8/354.

Wang, D. J., M. Mookherjee, Y. S. Xu, and S. I. Karato (2006), The effect of water on the electrical conductivity of olivine, *Nature*, *443*, 977–980, doi:10.1038/nature05256.

Wang, D. J., H. P. Li, L. Yi, and B. P. Shi (2008), The electrical conductivity of upper-mantle rocks: Water content in the upper mantle, *Phys. Chem. Miner.*, *35*, 157–162, doi:10.1007/s00269-007-0207-1.

Wenden, H. E. (1957), Ionic diffusion and the properties of quartz, *Am. Mineral.*, *42*, 859–888.

Xu, M. Y., H. Jain, and M. R. Notis (1989), Electrical properties of opal, *Am. Mineral.*, *74*, 821–825.

Xu, J., Y. Zhang, and W. Hou (1994), Measurements of ultrasonic wave velocity at high temperature and high pressure for window glass pyrophyllite and kimberlite up to 1400°C and 5.5 GPa, *High Temp. High Pressures*, *26*, 375–384.

Xu, Y. S., et.al. (2000a), A review on the electrical conductivity of mantle minerals and rocks, *Earth Sci. Front.*, *7*, 229–237.

Xu, Y. S., T. J. Shankland, and A. Duba (2000b), Pressure effect on electrical conductivity of mantle olivine, *Phys. Earth Planet. Inter.*, *118*, 149–161, doi:10.1016/S0031-9201(99)00135-1.

H. Li and D. Wang, Laboratory for Study of the Earth's Interior and GeoFluids, Institute of Geochemistry, Chinese Academy of Sciences, 46 Guanshui Rd., Guiyang, Guizhou 550002, China. (duojunwang@hotmail.com)

L. Yi, Institute of Earthquake Science, China Earthquake Administration, No. 63 Fuxing Ave., Beijing 100036, China.

T. Matsuzaki and T. Yoshino, Institute for Study of the Earth's Interior, Okayama University, 827 Yamada, Misasa, Tottori 68200193, Japan.